

## Path to turbulence in a transitional asymmetric planar wake

Jean-Pierre Hickey<sup>1</sup> and Khaled Younes<sup>1</sup>

*Department of Mechanical and Mechatronics Engineering, University of Waterloo,  
Ontario, Canada*

(Dated: 6 September 2019)

We report on a transitional, high-resolution direct numerical simulation (DNS) of a temporally developing planar asymmetric wake at  $Re = 4000$  based on the mass flux deficit. The asymmetric wake is formed by a Blasius and a fully-turbulent boundary layer on either side of an infinitely thin splitter plate. Such a setup has direct relevance in low-Reynolds number aeronautics where pressure gradients on an aerofoil can relaminarize transitional wall-bounded flows, thus generating a half-laminar/half-turbulent wake. The spreading and normalized turbulence intensity of the asymmetric wake are lower than the initially fully laminar wake but greater than the initially turbulent wake. In the far-field, the flow reaches a fully symmetric and nearly self-similar state with a high level of structural organization, originating from the transition of the laminar side. The structures are generated by the mutual interaction of the turbulent/laminar half-wakes. A forcing from the turbulent side accelerates the development of spanwise-organized structures on the laminar side, which evolve and develop a high-level of spanwise coherence. Unlike the classical transitioning wakes, the pairing of the roller is bypassed. Instead, the spanwise-aligned bulges appear from the initially turbulent half-wake. Under the local shear of the Blasius boundary layer, these bulges undergo a ‘kinking-and-stretching’ mechanism similar to the mixing layer. The spanwise organization of the structures is maintained far downstream.

PACS numbers: Valid PACS appear here

Keywords: wake, transition

## I. INTRODUCTION

The study of canonical free shear flows remains of fundamental interest to the fluid dynamics community. The inherent simplicity of these flows gives us an opportunity to gain a better understanding of the flow physics, abstracted from near-wall turbulence effects. Despite that, important scatter in the normalized turbulence statistics can be observed between various investigations. The scatter contradicts Townsend's<sup>1</sup> idea that the far-field statistics eventually reach a universal state that is independent of the near-field. To explain these differences, George<sup>2</sup> suggested the possibility of multiple self-similar states which depend on the initial conditions of the flow.

For the case of the planar wake, experimental<sup>3,4</sup> and numerical<sup>5</sup> works have highlighted the indelible ‘memory’ of the generating bodies of the wakes. For the specific case of the flat-plate wake, Bonnet *et al.*<sup>6</sup> showed that the boundary layer state at the trailing edge strongly modifies the turbulence statistics, spreading, and structures in the far-wake. The influence of the boundary layer state can be illustrated by a simple conceptual model: in the wake of an initially turbulent splitter plate, the flow develops through the cross-correlation of two statistically independent flow fields (on either side of the generating body), whereas in the laminar case, the structures are related to the instability modes of the velocity profile. This idea was further investigated using direct numerical simulations by Hickey *et al.*<sup>7</sup> They showed that the negative cross-wake velocity correlation was maintained in the far-field when the planar wake was generated by initially turbulent boundary layers. For an initially laminar wake, a slightly positive cross-wake velocity correlation was observed, supporting the findings in<sup>6</sup>. Interestingly, the wake composed of an initially turbulent and an initially laminar boundary layer, denoted here as an asymmetric wake, took on characteristics similar to a fully turbulent wake in the far-field. **As the turbulence characteristics of the fully laminar and fully turbulent wakes are drastically different in the near field, yet the asymmetric wake evolves similar to a fully turbulent wake in the far-field, this may have some implications in the dissipation scaling used to collapse the data (see, e.g. the work of Nedic *et al.*<sup>8</sup>).**

The asymmetric wake has direct relevance to the study of low-Reynolds number aerofoils, as the pressure gradients can greatly influence the state of the boundary layer at the trailing edge. The negative pressure gradient on the lift side can promote relaminarization of the boundary layer, whereas, the adverse pressure gradient on the suction side maintains

the turbulent boundary layer. As the streams merge, the laminar and turbulent half-wakes mutually interact and the subsequent evolution differs from either the fully laminar or fully turbulent wakes. Experimental work on an idealized asymmetric wake was carried out by Thomas and Liu<sup>9</sup>, who noted a drift of the centerline location and the inability of the Reynolds stresses to reach a self-preserving state. Furthermore, they noted a higher spreading rate than fully turbulent wakes. A clear explanation of the observed phenomena and the applicability of these findings to the far-wake remains unanswered by their work. More recently, experimental work by Kim *et al.*<sup>10</sup> investigated the Reynolds stresses in the near-field of an asymmetric wake of a bluff-body and showed a strong dependence on the upstream conditions. A similar setup was investigated using a spatially developing direct numerical simulation by Rai<sup>11</sup>. Although the aforementioned works provide comparative benchmark cases, bluff-body effects make the physical understanding of the transition process difficult to isolate. Asymmetric bluff-body wakes can also be generated by rotating cylinders; a review of the transition of such flows is found in<sup>12</sup>. Hickey *et al.*<sup>7</sup> studied the far-field evolution of an asymmetric wake at a Reynolds number of  $Re = 1500$  based on the mass flux deficit, until an approximate self-similar state was achieved. They contrasted the far-field evolution of the asymmetric wake with a transitional wake and a fully turbulent wake. Wu and Hickey<sup>13</sup> qualitatively studied an asymmetric wake in the context of turbine cascades. Finally, recent work by Dghim *et al.*<sup>14</sup> experimentally investigated the development of the wake from asymmetric shear layers. The exact structural characteristics of the flow in the asymmetric wake, especially in the near-wake, and the connection to the far-field evolution remains unclear however.

To understand the transition mechanism of the initially laminar half-wake, we recall the main features of the fully laminar wake transition. The inflection point in the velocity profile causes the wake to be unstable to any perturbation<sup>15</sup>. The Kelvin-Helmholtz (KH) instability develops into large spanwise rollers, with opposite vorticity on either side of the centerplane, that are connected through streamwise inclined braids<sup>16,17</sup>. Once the energy content of the principal instability mode is saturated, the rollers pair and the wake undergoes a rapid lateral spreading before eventually reaching a self-preserving state. In the case of the asymmetric wake, very little is known about the mechanism by which the laminar side becomes fully turbulent. The central question that remains to be answered is whether the laminar side becomes turbulent through a KH-type instability, through entrainment of

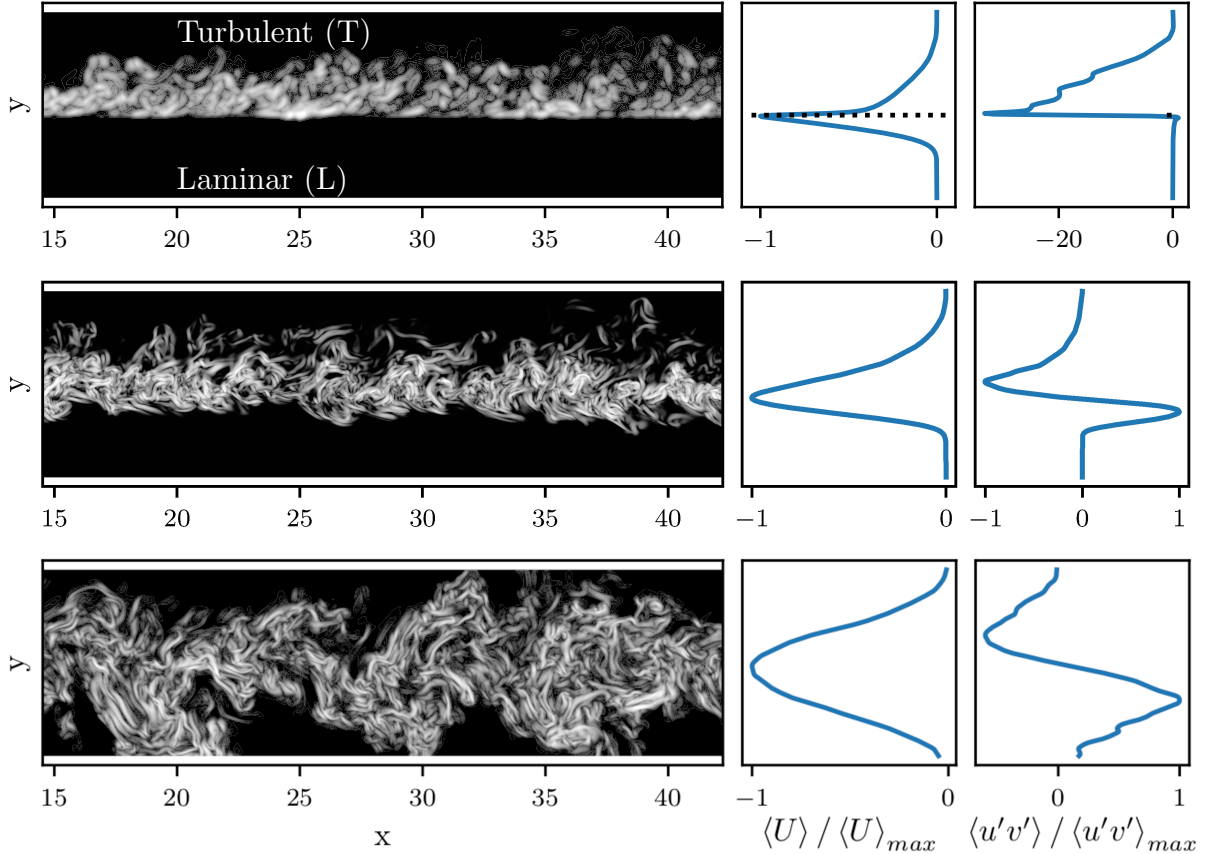


FIG. 1. Snapshot of the setup in the near-wake evolution. The contours of the vorticity magnitude are shown at  $z = 5$  (left) with the streamwise average velocity  $\langle U \rangle$  and vorticity magnitude  $\langle u'v' \rangle$  profiles (right). The snapshots are at  $t = 2, 19$ , and  $60$ , respectively, from top to bottom.

the turbulent side, or through another bypass-type mechanism. To answer this question, we first present the details of our direct numerical simulation. Then, we analyze the far-field statistics and show the evolution of the flow towards self-similarity. Thereafter, we study the transitional statistics in the transitional region. More specifically, we study the Reynolds stresses and total enstrophy, plot two-point velocity correlation maps, and perform a quadrant analysis in the transitional region. We also break down the mass and momentum transport across the wake centerplane to identify the dominant turbulence events occurring during transition. Finally, based on instantaneous visualizations of the near-wake flow field, a transition mechanism for the laminar side of the wake is proposed.

## II. NUMERICAL DETAILS

We simulate a temporally evolving asymmetric wake with direct numerical simulation using an in-house code. The code was extensively validated against analytical and canonical flows<sup>7,18–20</sup>. We solve the full, compressible Navier-Stokes equations in conservative form. However, we compute the skew-symmetric form of the convective terms to ease the aliasing problems caused by the high-order non-linearities. We close the conservation equations (mass, momentum, energy, and passive scalar) by using the ideal gas equation of state to relate the pressure to the thermodynamic properties of the flow. A fourth-order MacCormack-like finite differencing scheme is used in conjunction with a fourth-order Runge-Kutta time integration. In the present work, we consider a nearly incompressible wake despite the use of a compressible solver. The initial relative Mach number based on the centerline velocity deficit is set at  $\text{Ma}=0.3$  and decays as the flow evolves in time. The maximum relative density fluctuation is on the order of  $\langle \rho' \rangle_{\text{max}} / \langle \rho \rangle \approx \mathcal{O}(10^{-5} - 10^{-7})$ . A similar order of magnitude is noted for other flow characteristics, such as the dilatation. This makes the flow incompressible for all essential purposes.

The laminar boundary layer on the lower side of the wake is constructed using a Blasius velocity profile. The upper side is initialized with a fully developed turbulent boundary layer taken from the investigation of Wu and Moin<sup>21,22</sup>. Their boundary layer computation consists of a spatially developing flow with periodically passing isotropic turbulence in the free stream. The turbulence intensity of the isotropic turbulence—which is well outside the laminar boundary layer—is 3%, sufficient to bypass any Tollmien-Schlichting instability modes. For the present simulation, the fully turbulent velocity field from the Wu and Moin simulation was centered at  $\text{Re}_\theta=1200$ . The density was assumed constant and local pressure fluctuations resulted in very slight changes in temperature. Within the first few time-steps, the flow field adapted to the compressible solver without generating erroneous results. Both laminar and turbulent wake halves are scaled to have identical mass flux deficit. The velocity at the centerplane is null at the initial time-step because of the imposed non-slip boundary condition on each of the boundary layers. A two-dimensional slice of the setup is shown in figure 1.

The temporally developing wake can be understood as a box moving with the free stream, where an infinitely thin splitter plate is instantaneously removed at the first time-step. This

setup avoids any trailing edge receptivity issues commonly experienced in spatially developing flows and allows for a study of the flow physics void of bluff-body effects. For a temporal simulation, the domain is periodic in both the streamwise (*x*-axis) and the spanwise (*z*-axis) directions. The cross-wake (*y*-axis) domain remains finite. A non-reflective Thompson<sup>23</sup> boundary condition is applied in conjunction with a sponge layer in the cross-wake direction. The sponge dampens any spurious oscillations that may occur at the boundaries due to the inviscid approximation of the characteristic lines of the primitive variables. As the free stream velocity is dynamically insignificant, the velocity is scaled by the initial centerplane deficit. The length scale is then a ratio of the mass flux deficit,  $m_d = \int_{-\infty}^{\infty} (U_{\infty} - \langle u(y) \rangle) dy$ , and the initial velocity deficit,  $U_d$ . As the flow is temporally evolving, we set the free stream velocity,  $U_{\infty}$ , to zero; the resulting velocity in the wake deficit is negative. Based on these parameters, the domain size is [75, 40, 20]. The grid is composed of over 715 million grid points ( $2048 \times 704 \times 496$ ), which allows for a resolution down to the Kolmogorov scale. The grid is homogeneously distributed in the periodic directions and a hyperbolic tangent mapping is used to cluster the grid points around the centerplane. The simulation was conducted on 64 dedicated SPARC64 VII (2.52 GHz) processors on a Sun Enterprise M9000 cluster, with a clock time of 4 months to achieve approximate self-similarity. The simulation was conducted in 2012 but the results have not yet been reported in the literature.

### III. RESULTS

In this section, we first present the statistical evolution of the asymmetric wake from its early stages and until it reaches the far-field. This allows us to contrast some of the differences observed with other canonical wake flows. We then investigate, from a detailed turbulence statistical point of view, the transition to turbulence in the asymmetric wake. Thereafter, we explain the transition mechanism based on the emergence of coherent structure. We also tie the structural interpretation with the statistical analysis. The results reveal a transition mechanism that bypasses the classical instability modes of the laminar wake. Further, it appears to be characterized by a forcing imposed from the turbulent half-wake.

We will be repeatedly referring to either the ‘laminar’ (*L*) or ‘turbulent’ (*T*) side of the wake herein; this constitutes the initial state of the half-wake as being either laminar (Blasius) or turbulent. In addition, the standard Reynolds decomposition is denoted as

$\phi(x, y, z, t) = \Phi(y, t) + \phi'(x, y, z, t)$ , and the temporal velocity is  $u(x, y, z, t) = U(y, t) + u'(x, y, z, t)$ , where  $U(y, t)$  is an averaged velocity field along the periodic domains  $(x, z)$  at time  $t$ . Finally, when necessary, the spatially averaged quantities are enclosed in brackets such as  $\langle u' u' \rangle$ .

### A. Statistical evolution towards the far-field

Through mathematical manipulation of the governing equations (see, e.g. Moser *et al.*<sup>5</sup>), we can show that the square of the wake half-width,  $b^2$ , grows linearly with time (or space); a relation which has been observed for different wake generating bodies<sup>3,4,17</sup>, initial conditions<sup>6,7</sup>, and levels of forcing<sup>5</sup>. Dairay *et al.*<sup>24</sup> and Cafiero and Vassilicos<sup>25</sup> have recently shown that under the assumption of non-equilibrium dissipation, new scaling laws can be derived. Figure 2 (left) shows how the asymmetric wake compares with classical low-Reynolds number scaling laws. It is encouraging to note that the current setup obeys similar relations. We would like to point out that the present simulations differ from those conducted by Hickey *et al.*<sup>7</sup> in two distinct ways: the size of the domain and the Reynolds number of the flow (their results are at  $Re = 1500$ ; our results are at  $Re = 4000$ ). In addition to obeying similar scaling laws, it is evident that the spreading rate of the asymmetric wake is larger than the initially unforced turbulent side, yet smaller than the fully laminar wake. This result corroborates and expands the findings in<sup>7,9</sup>. Interestingly, the two asymmetric wakes (at  $Re = 1500$ <sup>7</sup> and  $Re = 4000$ ) have an identical spread rate. This finding differs from bluff-body transitioning wakes in which the flow statistics are particularly sensitive to the Reynolds number in the region of  $Re = \mathcal{O}(10^2 - 10^4)$ <sup>26</sup>.

The asymmetry of the current setup is more clearly illustrated in the evolution of the mean flow profile (figure 2 (right)). The location of the maximum deficit drifts from the centerplane to the laminar side of the wake during the preliminary stages of transition; a similar observation was noted by Thomas and Liu<sup>9</sup>. The shift reaches a maximum of 14% of the wake half-width. As the flow evolves, the centerline is slowly regained and symmetry is achieved. We attribute the drift to the differing mean velocity gradients and turbulence intensities on either side of the wake centerplane. On the turbulent side, there is a rapid kinetic energy transfer caused by high levels of turbulent fluctuations. The turbulent energy transfer results in an acceleration of the centerline velocity (reducing the centerline deficit)

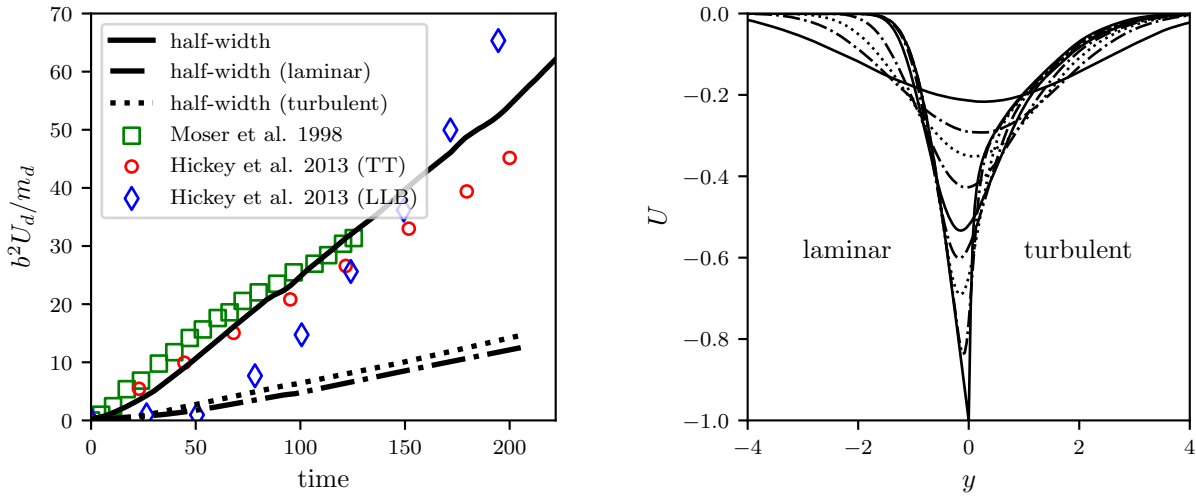


FIG. 2. Left: Evolution of the spreading rate; the individual wake half-width for each side of the laminar and turbulent half-wakes is also shown. Comparative results are shown from<sup>5</sup> and<sup>7</sup> for the fully turbulent (TT) and initially fully laminar with Blasius profile (LLB) wakes. Right: Changes to the mean streamwise velocity profile. From bottom to top along the centerline, the curves correspond to times  $t = 0, 5, 10, 16, 20, 30, 45, 60$ , and  $94$ , respectively.

and a deceleration of the outer wake. On the laminar side and in the absence of turbulent mixing, the flow near the centerline does not undergo the same acceleration as the kinetic energy is transferred solely by viscosity. As the entire wake becomes fully turbulent and large scale coherent structures form, turbulent kinetic energy production on the laminar side surpasses that of the originally fully turbulent side, **the maximum deficit drifts back to the wake centerline, and symmetry is reached in the far-wake.**

Despite the large scale events, when properly scaled, the mean velocity profile collapses with classical wake data as shown in figure 3 (left). Similarly, the turbulent fluctuations show an approximate symmetry with respect to the centerplane in the far-wake and evolve with a nearly self-similar profile; these results compare well with the experimental results of Thomas and Liu<sup>9</sup>. Finally, through a scaling based on the non-equilibrium dissipation assumption, as proposed in<sup>24,25</sup>, a near self-similar evolution in the far-field is further confirmed (results not shown).

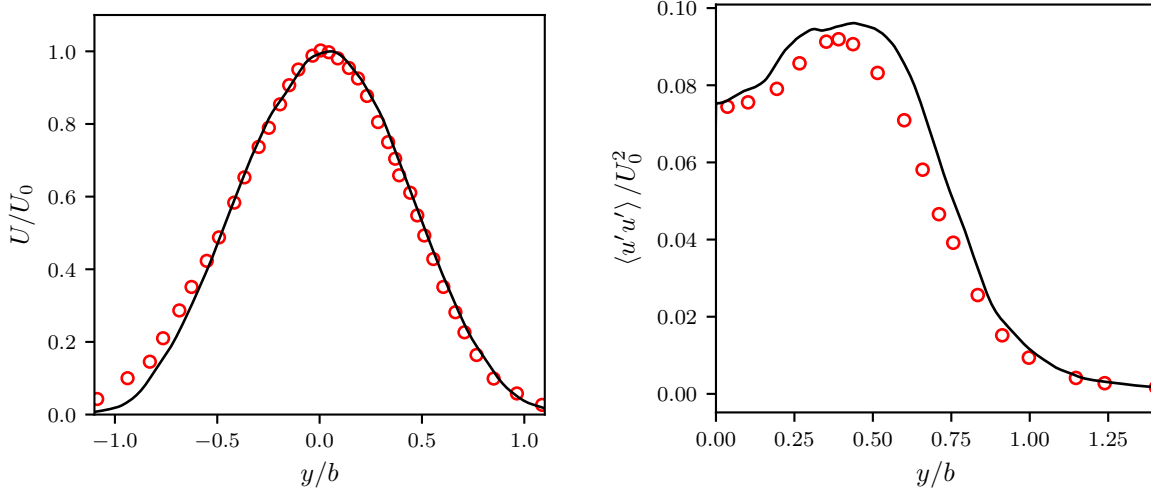


FIG. 3. Left: Scaled mean streamwise velocity profile in the self-similar region. Right: Scaled second-order statistics in the self-preserving region. Red circles represent the experiments in<sup>9</sup>.

## B. Transition to turbulence

This section focuses on the early evolution of the asymmetric wake to investigate the effect of the turbulent half-wake on the initially laminar half-wake. The following subsections address the evolution of the turbulence statistics, structures, quadrant analysis, and mass and momentum transport across the centerplane.

### 1. Turbulence statistics

Figure 4 (left) shows the near-field evolution of the spatially averaged Reynolds stresses, plotted on a logarithmic scale. As turbulent structures develop, a global maximum occurs at about  $t = 5, 10$ , and  $30$  for  $\langle u'u' \rangle$ ,  $\langle v'v' \rangle$ , and  $\langle u'v' \rangle$ , respectively. The emergence of a peak Reynolds stress is consistent with the behaviour of a fully turbulent or a transitional planar wake. Yet, a clear secondary peak in both Reynolds stresses,  $\langle u'u' \rangle$  and  $\langle v'v' \rangle$ , appears at  $t \approx 25$ . Until then, peak turbulence values were located on the initially turbulent side of the wake. At  $t \approx 25$ , the peak value shifts to the initially laminar side of the wake, signifying the emergence of coherent structures in the late transitional stage. The evolution of the normalized  $\langle u'u' \rangle$  profile is shown in figure 4 (right). To highlight the differences on either side of the wake, we normalize the profiles at each time-step by the maximum value,

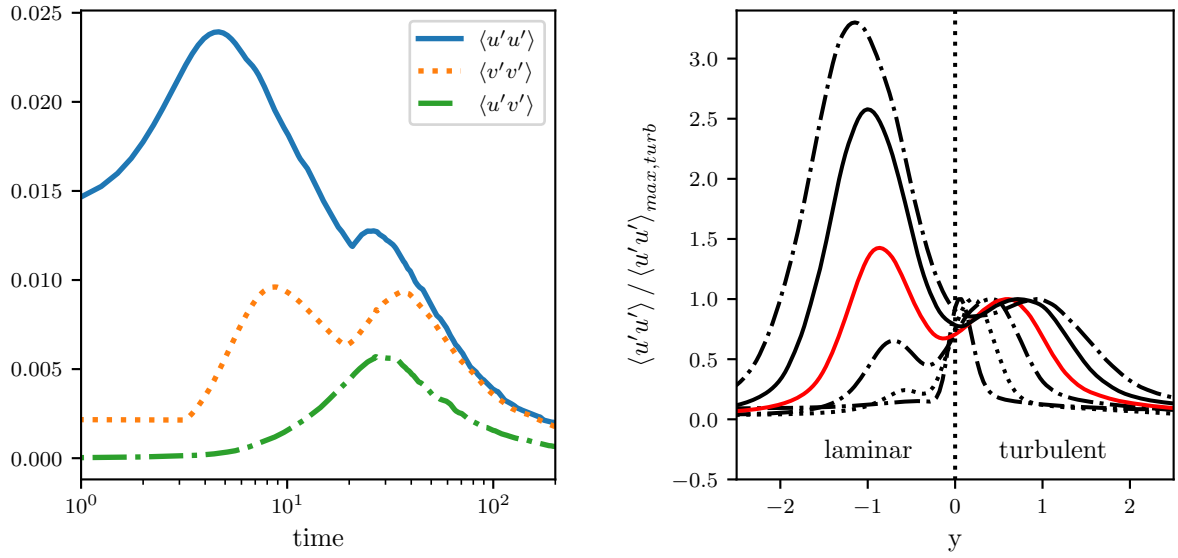


FIG. 4. Left: Time evolution of the maximum turbulent stresses  $\langle u'u' \rangle$ ,  $\langle v'v' \rangle$ , and  $\langle u'v' \rangle$ . Right: Profiles of the normalized  $\langle u'u' \rangle$  at times  $t = 5, 10, 15, 20, 25$ , and  $30$  from bottom to top, respectively. The red solid line corresponds to  $t = 20$  and represents the first location in which  $\langle u'u' \rangle$  on the laminar side surpasses that of the turbulent side.

$\langle u'u' \rangle_{max}$ , found on the turbulent side. A rapid increase in streamwise turbulent fluctuations is noted on the laminar side between  $t = 20 - 25$ , coincident with the secondary peak in the Reynolds stresses. From this, we can infer that on the initially laminar side of the wake, the structural development is delayed and that the secondary peak in the maximum Reynolds stresses is correlated with the development of coherent structures.

Next, we study the enstrophy of the flow (figure 5). Enstrophy, defined as  $E(\omega) = \int_V |\omega|^2 dV$ , provides a quantitative measure of the vortical activity and is widely associated with the turbulent kinetic energy dissipation<sup>27</sup>. As with the Reynolds stresses evolution, enstrophy initially peaks on the turbulent side (at  $t \approx 10$ ) and then monotonically decays. Following the decay, the enstrophy of the laminar half-wake shows a rapid increase with a delayed peak spanning  $t = 20 - 50$ . The total enstrophy in the entire flow, the sum of both half-wakes, has a singular peak.

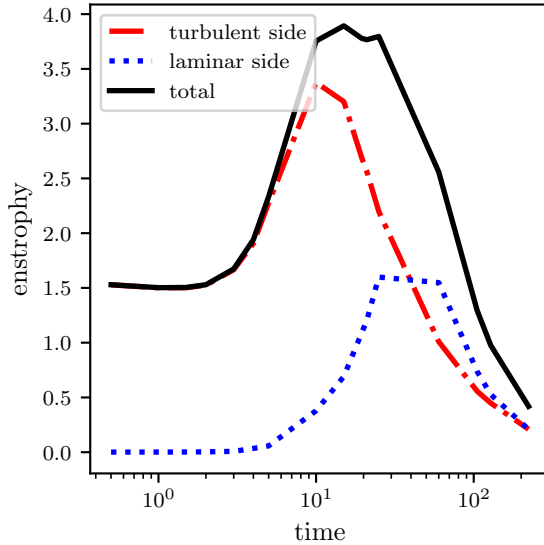


FIG. 5. Evolution of the total enstrophy in the asymmetric wake. The contributions from the initially laminar and turbulent sides are shown for reference.

## 2. *Structures and two-point correlations*

The turbulent statistics and enstrophy provide integral measures of the turbulent structures emerging during transition. To better characterize the structural development, however, two-point correlation maps of velocity fluctuations are insightful. Figure 6 plots such maps at characteristic locations in the wake. The fixed point is taken at the wake half-width on the turbulent side ( $dy = 0.5$ ); the centerplane is located at  $dy = 0$ . We note a strong cross-wake velocity correlation emerging at a very early stage of transition ( $t < 2$ ) and extending throughout the entire wake. Such a strong correlation would not be expected if the laminar half-wake were to transition via an intrinsic inflectional instability. Thus, this finding reveals that the transition of the laminar side is a direct result of a forcing by the turbulent half-wake. The characteristic wavelength of the emerging structures during transition can be inferred from the cross-wake velocity correlation. At  $t = 10$ , the characteristic wavelength normalized by the wake half-width is  $\lambda = 1.75$ ; at  $t = 25$ , the wavelength is  $\lambda = 4$ . The characteristic wavelength continues to increase, albeit very slightly, into the far-field.

From figure 6, we also note a high level of coherence in the early stages of transition. A

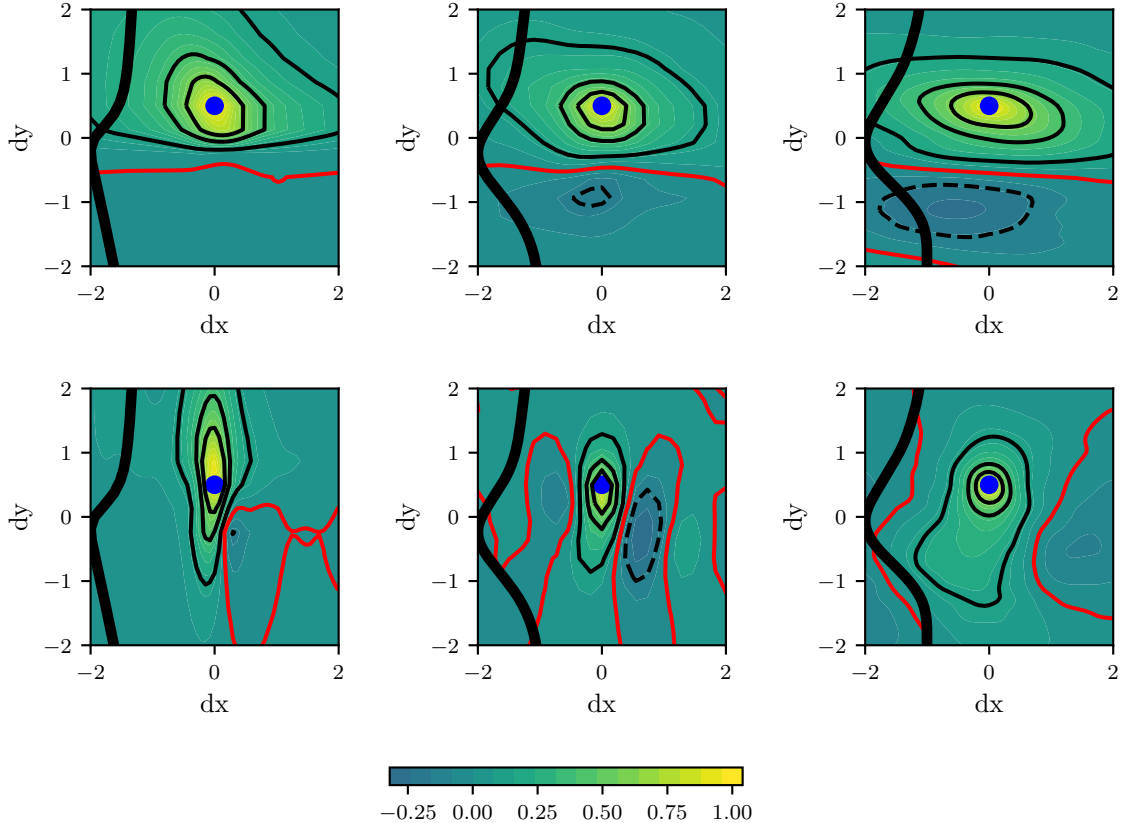


FIG. 6. Streamwise (top row) and cross-wake (bottom row) two-point velocity correlation maps at the wake half-width of the initially turbulent side ( $dy = 0.5$ ) at  $t = 2, 10$ , and  $25$  from left to right, respectively. The spatial coordinates are normalized by the wake half-width. The mean velocity profile is shown for reference (thick black line). The black contour lines are at a correlation coefficient of:  $-0.15$  (dashed line),  $0.15$ ,  $0.4$ ,  $0.6$ , and  $1$ . The red contour line corresponds to the boundary between positive and negative correlations.

correlation coefficient of  $-0.5$  is computed for the streamwise velocity at  $t \approx 6$ ; the minimum correlation coefficient drops to  $-0.2$  in the later stages of transition ( $t > 20$ ). This change underscores the importance of organized coherent structures in the transition of asymmetric wakes. Similar to the observations in Hickey *et al.*<sup>7</sup>, we observe that the emerging structures in the transitional asymmetric wake are highly organized and span nearly the entire height of the wake. **This finding lends support to a bypass-like transition as the normal instability mode of a wake is characterized by the well-known vortex street.**

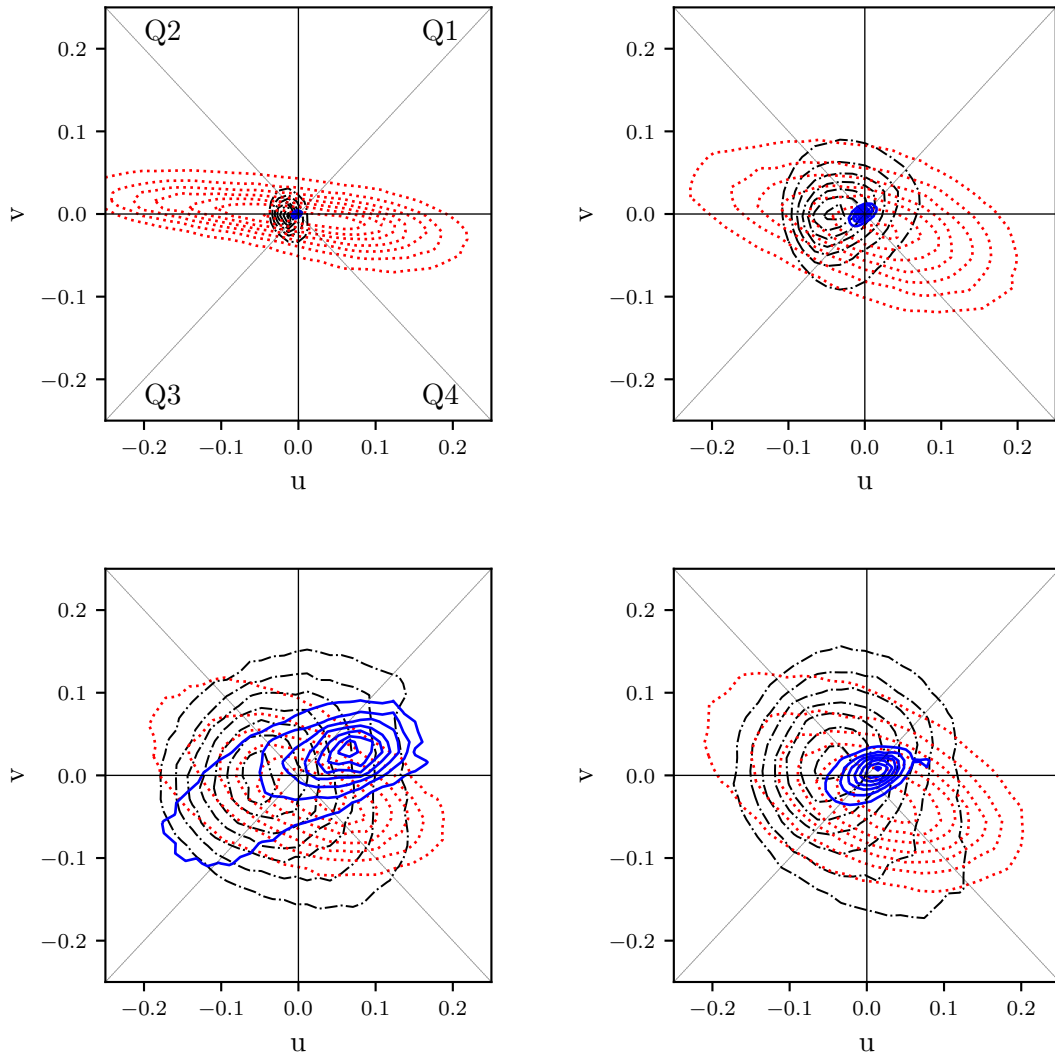


FIG. 7. Quadrant analysis of the streamwise and spanwise fluctuations at the centerline (dot dashed line, black), initially turbulent half-wake (dotted line, red), and initially laminar half-wake (full line, blue) at times  $t = 2, 5, 10$ , and  $20$  clockwise from top left.

### 3. Quadrant analysis

As the structural make-up of the transition can be informed by correlation maps, the impact of these structures on the dynamics of transition can be best understood through a quadrant analysis. The premise of the quadrant analysis is to investigate the dominant turbulence events taking place at various stages of the transition process. We construct a joint probability distribution function,  $PDF$ , of the fluctuating quantities,  $u'$  and  $v'$ . In

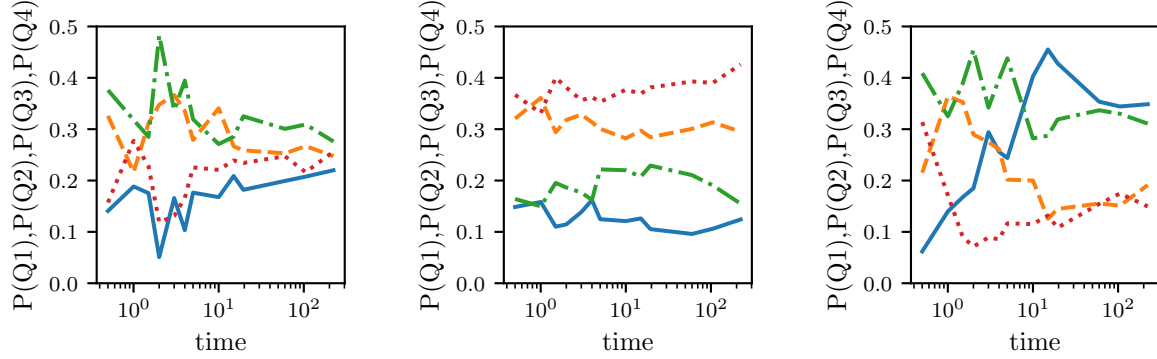


FIG. 8. Time evolution of the probability of occurrence of each quadrant at the centerplane (left), wake half-width of the initially turbulent side (center), and wake half-width of the initially laminar side (right). The lines correspond to quadrants Q1 (full line, blue), Q2 (dashed, orange), Q3 (dot dashed, green), and Q4 (dotted, red).

wall-bounded flows, the dominant turbulent stresses are caused by ejections ( $u' < 0$  and  $v' > 0$ ) and sweeps ( $u' > 0$  and  $v' < 0$ ), which are found in the second (Q2) and fourth (Q4) quadrants, respectively. Figure 7 evaluates the joint PDF at three key locations in the wake, namely: along the centerplane, at the wake half-width of the turbulent side, and at the wake half-width of the laminar side.

At the centerplane, the joint PDF has a slight bias towards the negative streamwise velocity fluctuation. This is surprising as we would typically expect that, in the absence of mean shear at the centerplane, a negative streamwise fluctuation would inherently be less probable than a positive fluctuation given that the minimum streamwise velocity is located at the centerline. We observe no bias with regards to the cross-wake velocity fluctuations,  $v'$ , even during transition. This is expected because the fluctuations in an isotropic flow evolve towards an isotropic state, with an equal probability of occurrence amongst all quadrants:  $P(Q1) = P(Q2) = P(Q3) = P(Q4)$ . Figure 8 (left) shows the time evolution of the probability of the four quadrants at the centerplane. An approximately equal probability is noted as  $t \rightarrow \infty$ .

At the wake half-width of the turbulent side, the flow evolves from a turbulent boundary layer-like joint PDF, with a shallow inclination of the primary axis of elliptical contour lines, to a fully developed wake flow. As expected, a greater probability of Q2 and Q4 events are observed. In the far-wake, both the initially laminar and turbulent half-wakes

have the major axis of the elliptical distribution aligned at around  $\pm 35$  degrees, similar to the expected inclination of the primary structures in the wake<sup>7</sup> (figure 7 (bottom left)).

At the wake half-width of the laminar side, we observe a high probability distribution of Q1 events. The anisotropic distribution is expected in the presence of spanwise coherent structures that are embedded within a mean shear. Given that the mean streamwise velocity gradient of the initially laminar half-wake has opposite signs to the turbulent half-wake, the sweep and ejection events are in Q1 and Q3, respectively. Interestingly, in the early stages of transition ( $t < 5$ ), we note a very high probability of Q4 ( $u' > 0$  and  $v' < 0$ ) events. This suggests that a transport of momentum from the turbulent half-wake takes place in the cross-wake direction; a similar observation is noted at the centerplane. As the flow evolves, the highest probability is distributed among the Q1 and Q3 quadrants (figure 8 (right)). It should be noted that large fluctuations in the quadrant distributions at the centerplane and laminar locations in the early stages of transition are due to the weak correlation present between  $u'$  and  $v'$  (see figure 4); the formation and growth of just a small number of organized structures can result in rapid changes in the joint PDFs. In the turbulent half-wake, we do not observe as large fluctuations.

#### ***4. Mass and momentum transport across centerplane***

The quadrant analysis suggests that a significant transport of momentum exists between the two half-wakes, especially during transition. It is thus clear that mass and momentum are central in addressing the potential forcing of the turbulent side on the laminar half-wake. The direct numerical simulation includes a scalar field that acts as a momentumless tracer. We compute the net transport of the scalar to either side of the wake. At the start of the simulation, the value of the tracer is set to unity at the centerplane, the distribution of the passive tracer is symmetric, and all the points above and below the centerpoint are initialized to zero. As the flows evolves, the scalar field is transported primarily by turbulence. Figure 9 shows this phenomenon pictorially using two-dimensional snapshots.

In figure 10, we plot the time evolution of the integrated scalar field on either side of the asymmetric wake. During the first stage of transition ( $t < 10$ ), we observe a significant increase in scalar transport from the turbulent side to the laminar half-wake. This is because the initially laminar half-wake does not contain any fluctuations; hence, no net mass or

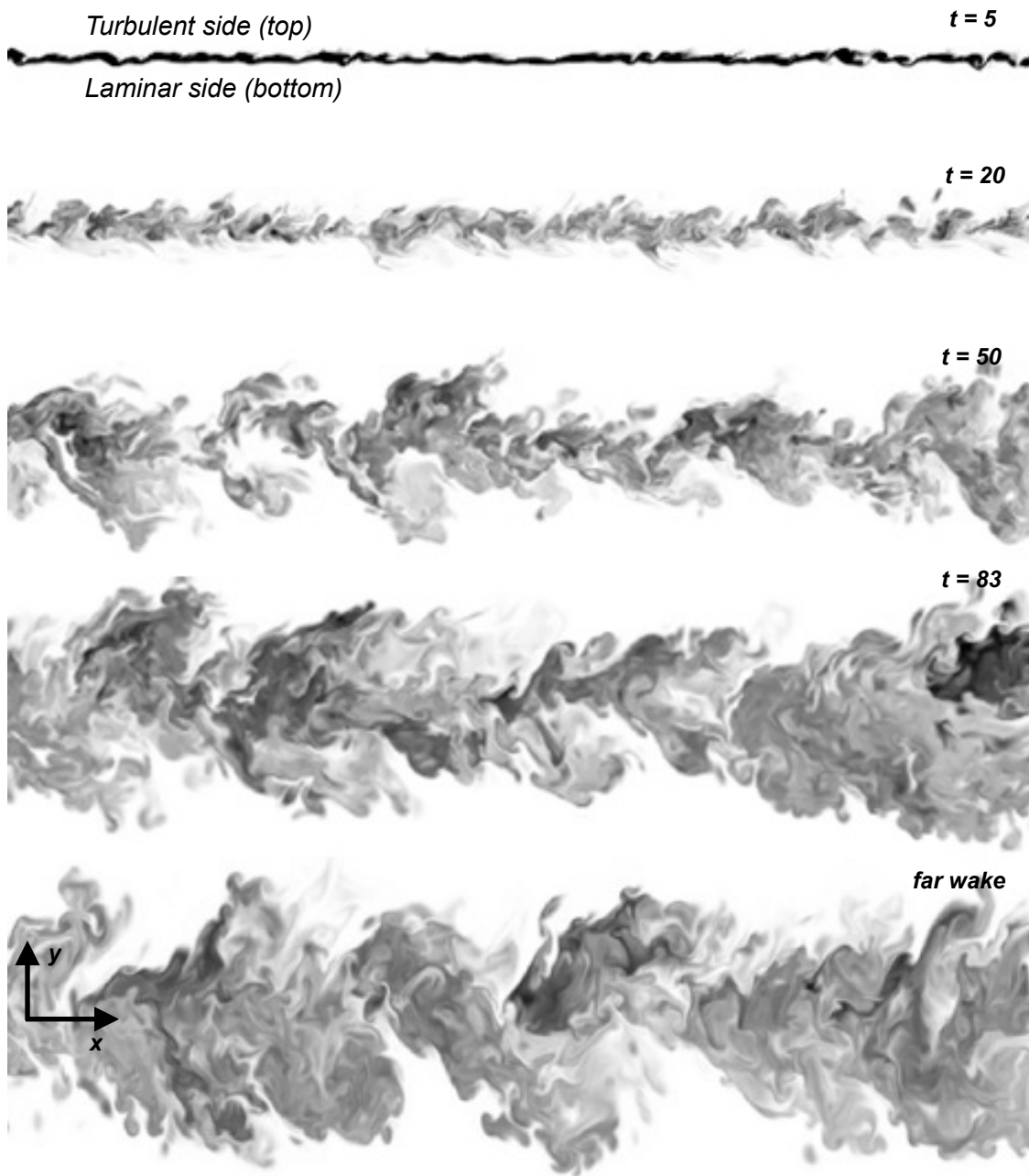


FIG. 9. Passive scalar at a randomly selected  $z$ -plane at times  $t = 5, 20, 50, 83$ , and far-wake from top to bottom, respectively. Flow is from left to right. The extent of the domain shown represents half the streamwise domain length.

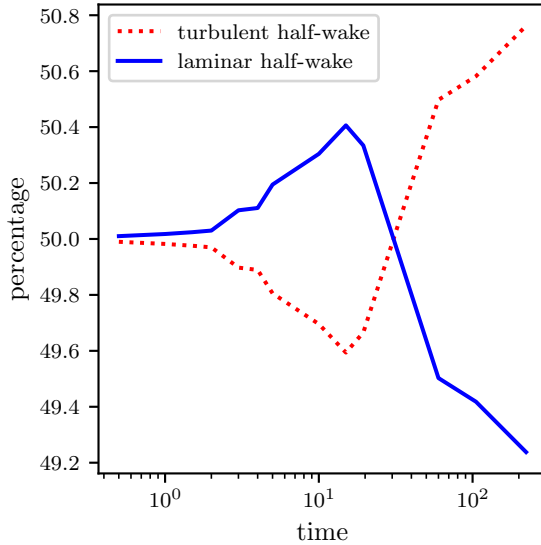


FIG. 10. Time evolution of the integrated scalar field on either side of the wake.

momentum transport is expected to the turbulent side. As the coherent structures in the laminar half-wake develop ( $10 < t < 20$ ) and the flow transitions ( $25 < t < 40$ ), we note reversed mass, and concomitantly momentum, transport from the initially laminar half-wake to the turbulent side. This can be attributed to the increased turbulent kinetic energy production on the laminar side caused by the emergence of highly organized coherent structures; this intense cross-wake transport is an important contributor to regaining the overall symmetry of the flow. The increased scalar transport to the initially turbulent side is maintained far into the wake evolution. *Although we did observe symmetric profiles and self-similar evolution in the far-wake, the tracers show a small increase in scalar transfer in the far-wake region. We hypothesize that this is caused by the memory effects of the flow and the anisotropic turbulent structures developing during transition.*

### C. Path to transition: structural perspective

The path to transition of the laminar side of the asymmetric wake is described in this section from a structural perspective. The evolution of the vorticity isosurface is shown in figure 11 for the laminar half-wake. Strong streaky structures, which recall features of the turbulent boundary layer, are found early in the transition at  $t < 3$ . As the transition

progresses, coherent structures emerge on the laminar side, confirming the findings from the turbulence statistics analysis. Figure 12 shows the isosurface of vorticity magnitude strictly in the laminar half-wake during transition. A clear shift from streamwise-aligned structures to a strong spanwise organization is observed during the early stages of transition. In fact, the observed vorticity ‘bulges’ can be traced back to the coherent structures of the initially turbulent side that protrude into the laminar half-wake. Interestingly, the bulges show a strong spanwise organization.

Given the appearance of these vortical bulges, figure 13 shows the evolution of the cross-wake velocity on the centerplane. It is evident that the presence of the vortical bulges is characterized, unsurprisingly, by local spots of negative cross-wake velocity. Additionally, it can be inferred that the vortical structures from the turbulent side create the localized cross-wake velocity seen in figure 6 at the centerplane. In figure 14, we follow the evolution of the spanwise structures in the laminar half-wake. Note that the structures are overlaid on a slice of spanwise vorticity. The vortex lines seem to form loops at certain locations in the wake, see figure 14 (last panel). This suggests that the legs of the hairpin-like structures in the turbulent boundary layer are combining. It is worth mentioning that the vortex loops are not observed everywhere in the flow. At other locations, we note that, despite the clear bulge into the laminar half-wake, loops are not observed and the vortex lines connect two neighboring coherent structures (figure 14 (second last panel)).

Based on these observations and through visualization of the  $\lambda_2$  isosurfaces<sup>28</sup>, we identify the sequence of events occurring during the transition of the laminar half-wake. First, it is well-known that: (a) the fully developed turbulent boundary layer is populated by hairpin-like structures with legs aligned in the streamwise direction<sup>21,22</sup>; these legs are characterized by high levels of streamwise vorticity, and, in turn, they create low-speed velocity streaks in the near-wall region, and, (b) vortex lines in free-shear flows must be continuous; only in the boundary layer can vortex lines terminate at the wall. In the asymmetric wake, the strict non-slip wall constraint ( $u, v, w = 0$  and  $\partial v / \partial y$  at  $y = 0$ ) is relaxed at the initial time step. Thus, it is possible for vortex lines to reconnect within a single hairpin (**forming a vortex loop**) or merge between neighboring hairpins, forming unusual coherent structures in the process. It should be noted that the sign of the spanwise vorticity at the centerplane remains the same under the formation of a vortex loop, self-connection of hairpin legs, or through the connection between the legs of neighboring hairpins. Both these events

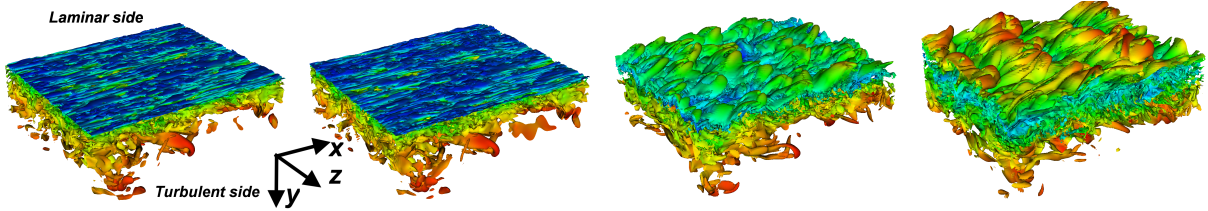


FIG. 11. Isosurface of vorticity magnitude colored by the instantaneous streamwise velocity at times  $t = 1.5, 5, 10$ , and  $20$  from left to right, respectively. The domain corresponds to  $10\%$  of the streamwise and spanwise extent.

have been observed in our simulation, as shown by the two left panels of figure 14. (The reconnection of neighboring hairpins and the formation of vortex loops was identified by investigating the vortex lines surrounding bulges at the centerplane.). Third, as the vortex loops (also called bulges) protrude through the centerplane into the laminar half-wake, they encounter a mean velocity gradient due to the original Blasius boundary layer profile. This causes the bulges to stretch out non-uniformly, yielding new streaky structures and hairpins. The process bears many similarities to the ‘kinking-and-stretching’ mechanism of the mixing layer proposed by Sandham *et al.*<sup>29</sup>

#### IV. CONCLUSIONS

The planar asymmetric wake—formed by an initially laminar half-wake and a turbulent boundary layer<sup>21,22</sup>—is studied using direct numerical simulation at  $Re = 4000$  based on the mass flux deficit. Despite the initial asymmetry, the wake eventually reaches a self-preserving state with scaling of first- and second-order statistics. The present study focuses on the transition to turbulence of the initially laminar half-wake. A quantification of the turbulence statistics reveals that the development of coherent structures in the laminar half-wake is delayed, despite the emergence of strong spanwise motion very early in the transition process. Two-point velocity correlation maps indicate that the turbulent side of the wake acts as a potential forcing on the initially laminar side. A quadrant analysis is conducted to identify the main events occurring during transition. Net mass and momentum transport from either half-wake is computed using a passive scalar. Significant transport from the turbulent to the laminar half-wake is noted prior to full transition; a reversal in

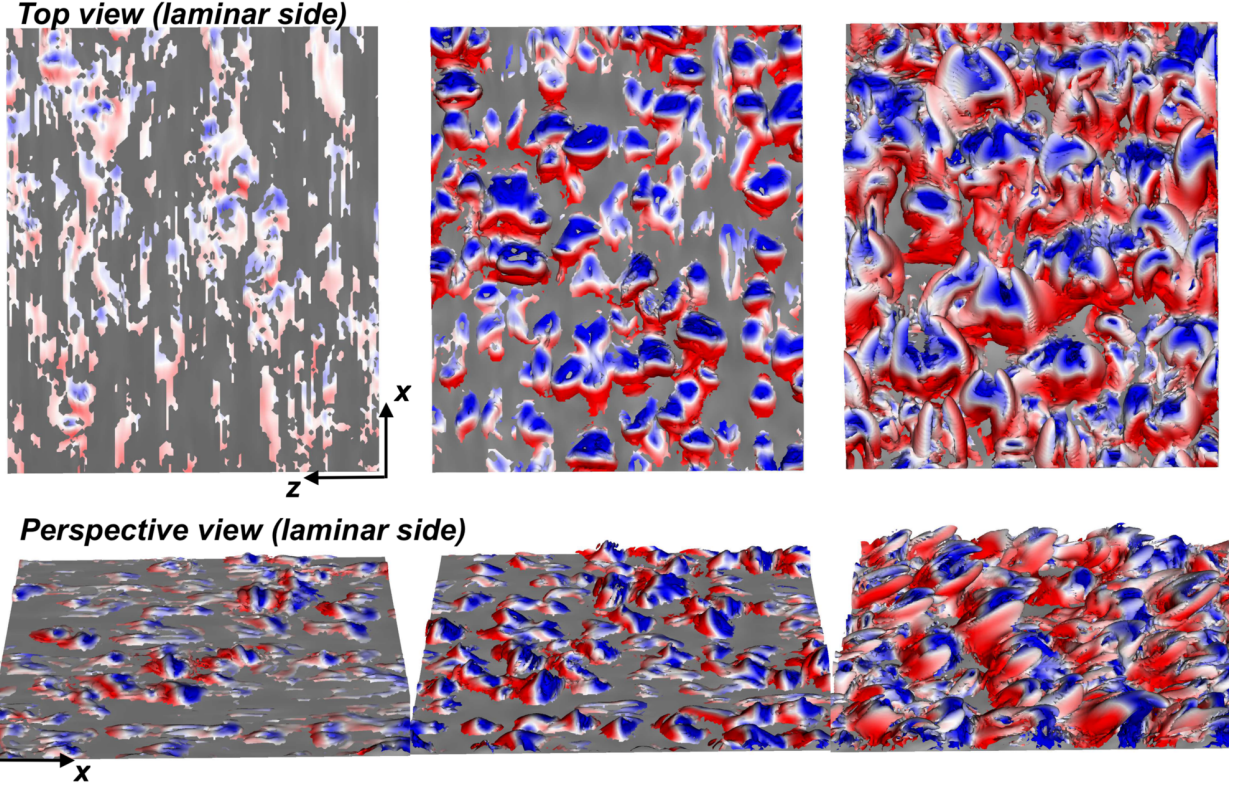


FIG. 12. Isosurface of vorticity magnitude below the centerplane (on the laminar side). Top view (top row) and perspective view (bottom row) at times  $t = 1.5, 3$ , and  $10$  from left to right, respectively. The structures are colored by the local cross-wake velocity (blue: into the page; red: out of the page).

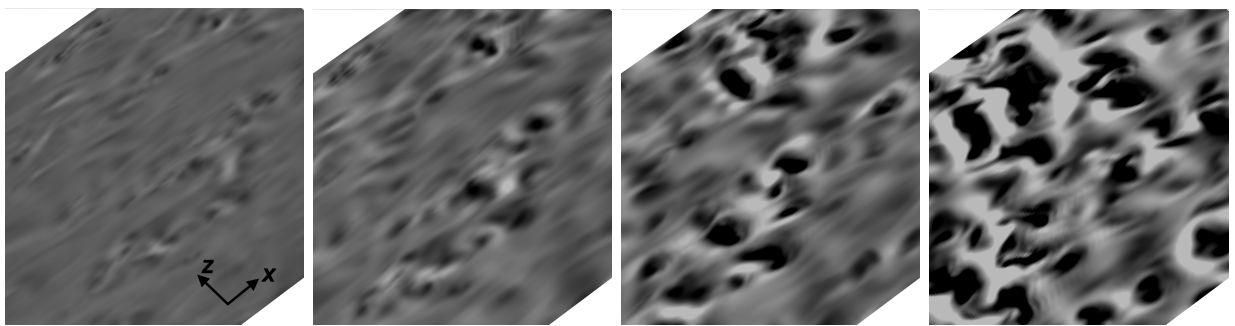


FIG. 13. Perspective view of the evolution of the cross-wake velocity on the centerplane of the asymmetric wake at times  $t = 0.5, 1.5, 3$ , and  $5$  from left to right, respectively. The dark regions correspond to motion directed towards the laminar side.

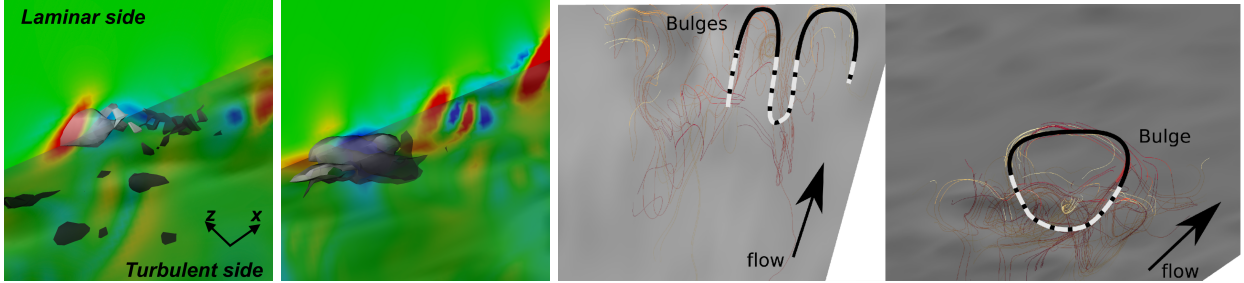


FIG. 14. Close-up on the isosurface of a single vortical bulge overlaid on a slice of spanwise vorticity at  $t = 3$  and  $t = 5$  (first two panels). Connection of vortex lines in adjacent hairpins and formation of a bulge in a self-connecting hairpin (second two panels).

the direction of transport is observed in the far-wake.

Through visualizations of the vorticity isosurfaces and  $\lambda_2$  contours, a transition mechanism is proposed for the laminar half-wake. **The transition mechanism is governed by turbulent forcing and starts** by the merging of the hairpin structures found on the turbulent side of the wake to form continuous vortex lines. This connection process arises within a single hairpin (vortex loop) and between two neighboring hairpins. The bulges resulting from this joining process are strongly spanwise-oriented and impinge on the laminar half-wake through the centerplane. Due to the Blasius construction of the laminar boundary layer, the bulges are accelerated preferentially yielding new streamwise oriented hairpin-like structures. In classical transitioning wakes, pairing of the Kelvin-Helmholtz rollers is normally observed. In the asymmetric wake, however, pairing of the rollers is not observed and is believed to have been completely bypassed. The flow setup studied in this report is highly relevant in low-Reynolds number airfoils, where negative pressure gradients on the lift side can promote relaminarization and adverse pressure gradients on the suction side maintain a turbulent boundary layer.

## ACKNOWLEDGEMENTS

We would like to acknowledge the financial support of the NSERC. This research was enabled in part by support provided by HPCVL (now called the Center for Advanced Computing), SciNet ([www.scinethpc.ca](http://www.scinethpc.ca)), and Compute Canada ([www.computecanada.ca](http://www.computecanada.ca)). An initial draft of this paper was presented at the Computational Fluid Dynamics Society of

Canada Meeting in June 2012 in Montreal, Quebec, Canada.

## REFERENCES

- <sup>1</sup>A. A. Townsend, J. Fluid Mech. **41**, 13 (1970).
- <sup>2</sup>W. K. George, *The self-preservation of turbulent flows and its relation to initial conditions and coherent structures*, edited by W. K. George and R. Arndt (Advances in Turbulence, Berlin, Springer, 1989) pp. 39–74.
- <sup>3</sup>L. Wygnanski, F. Champagne, and B. Marasli, J. Fluid Mech. **168**, 31 (1986).
- <sup>4</sup>Y. Zhou and R. A. Antonia, Exp. Fluids **19**, 112 (1995).
- <sup>5</sup>R. D. Moser, M. M. Rogers, and D. W. Ewing, J. Fluid Mech. **367**, 255 (1998).
- <sup>6</sup>J. P. Bonnet, J. Delville, and H. Garem, Exp. Fluids **4**, 189 (1986).
- <sup>7</sup>J.-P. Hickey, F. Hussain, and X. Wu, J. of Fluid Mech. **731**, 312 (2013).
- <sup>8</sup>J. Nedić, J. C. Vassilicos, and B. Ganapathisubramani, Phys. Rev. Lett. **111**, 144503 (2013).
- <sup>9</sup>F. O. Thomas and X. Liu, Phys. Fluids **16**, 1725 (2004).
- <sup>10</sup>D. H. Kim, J. Chang, H. Kim, and M. Sohn, Aerosp. Sci. Technol. **14**, 49 (2010).
- <sup>11</sup>M. Rai, in *AIAA 40th Fluid Dynamics Conference and Exhibit (AIAA 2010-4602)* (2010).
- <sup>12</sup>A. Rao, A. Radi, J. Leontini, M. Thompson, J. Sheridan, and K. Hourigan, J. Fluid Struct. **53**, 2 (2015).
- <sup>13</sup>X. Wu and J.-P. Hickey, AIAA Journal **50**, 215 (2012).
- <sup>14</sup>M. Dghim, L. Momayez, M. Ferchichi, and H. Peerhossaini, Heat Transfer Engineering , 1 (2017).
- <sup>15</sup>H. Sato and K. Kuriki, J. Fluid Mech. **11**, 321 (1961).
- <sup>16</sup>E. Meiburg and J. Lasheras, Phys. Fluids **30**, 623 (1987).
- <sup>17</sup>M. Hayakawa and F. Hussain, J. Fluid Mech. **206**, 375 (1989).
- <sup>18</sup>J.-P. Hickey, *Direct simulation and theoretical study of sub-and supersonic wakes*, Ph.D. thesis, Royal Military College of Canada (2012).
- <sup>19</sup>J.-P. Hickey and X. Wu, AIAA Journal **53**, 3821 (2015).
- <sup>20</sup>J.-P. Hickey, F. Hussain, and X. Wu, J. Fluid Mech. **796**, 5 (2016).
- <sup>21</sup>X. Wu and P. Moin, J. Fluid Mech. **630**, 5 (2009).
- <sup>22</sup>X. Wu and P. Moin, Phys. Fluids **22**, 085105 (2010).

- <sup>23</sup>K. W. Thompson, J. Comput. Phys. **68**, 1 (1987).
- <sup>24</sup>T. Dairay, M. Obligado, and J. C. Vassilicos, J. Fluid Mech. **781**, 166195 (2015).
- <sup>25</sup>G. Cafiero and J. Vassilicos, Proceedings of the Royal Society A **475**, 20190038 (2019).
- <sup>26</sup>H. J. Oertel, Annu. Rev. Fluid Mech. **22**, 539 (1990).
- <sup>27</sup>Y. Zhu and R. Antonia, Applied scientific research **57**, 337 (1996).
- <sup>28</sup>J. Jeong and F. Hussain, J. Fluid Mech. **285**, 69 (1995).
- <sup>29</sup>N. D. Sandham and R. D. Sandberg, J. Turbul. **10-1**, 1 (2009).